PHYSICAL REVIEW A VOLUME 36, NUMBER 8 OCTOBER 15, 1987

Electron-N_2 scattering calculations with a parameter-free model polarization potential

Michael A. Morrison and Bidhan C. Saha
Department of Physics and Astronomy, University of Oklahoma, Norman, Oklahoma 73019

Thomas L. Gibson
Department of Physics and Engineering Physics, Texas Tech University, Lubbock, Texas 79409
(Received 11 May 1987)

We have extended our variationally determined nonadiabatic polarization potential [Gibson and Morrison, Phys. Rev. A **29**, 2497 (1984)] to the e-N_2 system and calculated elastic, total momentum transfer, and rotational excitation cross sections. This model potential, which requires no scaling and contains no adjustable parameters, is presented in tabular and analytic (fitted) form for possible use in future studies. We evaluated the static potential at the near-Hartree-Fock level of accuracy and included exchange effects exactly via the linear algebraic method of Collins and Schneider [Phys. Rev. A **24**, 2387 (1981)]. Diverse cross sections based on this model are in excellent agreement with existing experiment. We also compare various scattering quantities calculated with our model to prior theoretical results and to newly determined numbers using two other model potentials: a cutoff phenomenological form and the correlation-polarization potential of O'Connell and Lane [Phys. Rev. A **27**, 1893 (1983)].

I. INTRODUCTION

Nitrogen is a much-studied molecule. For decades, theorists have probed the structure and spectra of N_2 as well as its behavior in a variety of scattering processes. Interest in electron collisions with this molecule is heightened by the importance of low-energy e-N_2 cross sections to such applications as gas discharge physics, laser kinetic modeling, and the physics of planetary atmospheres.[1] The low-energy ($\sim$2.4 eV) shape resonance,[2] which induces a rich oscillatory structure in e-N_2 cross sections, plays a significant role in such applications as the energetics of the CO_2-N_2 laser and has been exhaustively studied via a host of theoretical methods.[3] Still, questions remain.

One of these concerns is how to include in a practical, accurate theoretical method for calculating e-N_2 cross sections the long-range polarization and allied short-range correlation effects. Together with the bound-free electrostatic interaction and the exchange effects that arise from antisymmetrization of the system wave function, these effects are responsible for the shape and magnitude of cross sections at energies of tens of eV or below (see Sec. II.4.b of Ref. 4). Formally speaking, including polarization effects seems straightforward: One simply includes all contributing closed (i.e., energetically inaccessible) electronic target states in the eigenfunction expansion of the electron-molecule wave function that reduces the many-body Schrödinger equation to an effective one-body problem. Practically speaking, however, this strategy leads to coupled scattering equations so complicated that they resist solution. The nature of the difficulty is, as noted by Schneider and Collins,[5] the "multiconfigurational nature of polarization," which "implies that even with the most sophisticated modern computers and numerical methods, the effect can only be handled in an approximate fashion."

So it is not surprising to find in the recent literature a flurry of activity on the problem of polarization, or to discover that much of this activity has focused on the e-N_2 system. Of particular importance are recent implementations of optical-potential methods, such as the linear-algebraic calculations of Schneider and Collins,[5] R-matrix studies such as that of Burke *et al.*,[6] and pseudostate techniques such as the Schwinger multichannel method.[7] These studies require sophisticated, computer-intensive matrix calculations predicated on expansions of the scattering function, the potential, or a Green's function.[8] Indeed, at the heart of these methods is the idea of representing short-range correlation and long-range polarization effects (at least in part) by a finite basis of square-integrable functions. Underlying most such studies published to date is the *rigid-rotator approximation,* which, by "freezing" the internuclear separation of the target at equilibrium, obviates the need for coupling of vibrational states or for fixed-nuclei calculations at many internuclear separations.

A different tack to the problem posed by polarization is to conjure up a model potential. In the early days, model polarization potentials were crude representations of the simple, well-known asymptotic dependence, with nonadiabatic effects mimicked by a spherically symmetric cutoff function that strived to approximate intermediate-range adiabatic effects and short-range nonadiabatic influences. Notably superior to these heuristic models—though less rigorously founded than, say, an optical potential—are polarization potentials determined using the linear vibrational method, such as

the e-H_2 potential of Lane and Henry,[9] the e-N_2 polarized-orbital potential of Onda and Temkin,[10] and the present model.[11] Free of parameters requiring adjustment to experimental cross sections, these models face only one major problem in their implementation: inclusion of nonadiabatic effects. Our solution to this conundrum, which gives rise to the so-called "better than adiabatic dipole" (BTAD) potential (see Sec. II), is to invoke the nonpenetrating approximation of Temkin.[12,13]

Yet another approximate solution to the problem of polarization is to join the known asymptotic form of the polarization potential to an analytic fit of a short-range free-electron-gas correlation potential. This is the strategy adopted by O'Connell and Lane[14] in their study of electron–rare-gas scattering and by Norcross and collaborators[15,16] in (rigid-rotator) electron-molecule scattering calculations for a variety of systems. In the absence of results from rigorously exact treatments of polarization, the accuracy of this or any other model must be assessed indirectly, e.g., by comparisons of cross sections from calculations based on different models and from experiments.

In the present paper, we report several such comparisons for our BTAD potential. The primary intent of this work is to extend our initial implementation of this model,[11] which was restricted to electron collisions with the (comparatively) simple two-electron H_2 target, to a more typical electron–small-molecule system. With its seven molecular orbitals of various symmetry, and its more acutely nonspherical interaction potential, the e-N_2 system is ideally suited for this purpose. Our grail is a tractable, easily extensible, parameter-free model polarization potential that one can use with confidence in quantitative studies of vibrational excitation of diatomic and polyatomic molecules.

After summarizing the essentials of the model and the scattering theory in Sec. II and the computational details in Sec. III, we compare various theoretical e-N_2 cross sections to recently measured data. To put this model into perspective, we also compare various scattering quantities calculated using our variational BTAD model with newly calculated results using two other widely adopted model potentials (a cutoff phenomenological potential and the correlation-polarization model) and to results of other recent *ab initio* studies. All of this appears in Sec. IV.

II. THEORY

A. Polarization potentials

The adiabatic polarization potential is defined to be the change in the total energy of the projectile-molecule system due to the distortion of the target charge distribution by the scattering electron. In our procedure, a more detailed account of which appears in Ref. 11, we use the linear variational method to determine the energy of the electron-molecule system, treating the projectile as an additional "nucleus" (of charge $-e$) that is fixed at the position of the scattering electron. These molecular structure calculations are carried out in a body-fixed reference frame[3,17,18] with the origin of (single-center) coordinates at the center of mass of the molecule and the z axis coincident with the internuclear axis. We shall denote the spatial coordinates of the molecular electrons, nuclei, and scattering electron in this reference frame by $\mathbf{r}_m$, $\mathbf{R}_\alpha$, and $\mathbf{r}_e$.

In the adiabatic approximation, the target molecular orbitals can *fully* relax in the presence of the *fixed* projectile at r_e. From these relaxed orbitals, we construct the "polarized" wave function of the target, $\psi_0^{(p)}(\mathbf{r}_m;\mathbf{r}_e,R)$. Thus, for a given internuclear separation R, the adiabatic polarization potential is simply the difference between $E_0^{(p)}$, the expectation value of the adiabatic Hamiltonian $\hat{\mathcal{H}}^A$ with respect to the polarized wave function of the target, and E_0, its counterpart for the undistorted ground-state wave function $\psi_0(\mathbf{r}_m;R)$. That is, with unperturbed energy

$$E_0(\mathbf{r}_e;R)=\langle \psi_0(\mathbf{r}_m;R)\,|\,\hat{\mathcal{H}}^A\,|\,\psi_0(\mathbf{r}_m;R)\rangle \tag{1}$$

and perturbed energy

$$E_0^{(p)}(\mathbf{r}_e;R)=\langle \psi_0^{(p)}(\mathbf{r}_m;\mathbf{r}_e,R)\,|\,\hat{\mathcal{H}}^A\,|\,\psi_0^{(p)}(\mathbf{r}_m;\mathbf{r}_e,R)\rangle\ , \tag{2}$$

the adiabatic polarization potential is

$$V_{\rm pol}^A(\mathbf{r}_e;R)=E_0^{(p)}(\mathbf{r}_e;R)-E_0(\mathbf{r}_e;R)\ . \tag{3}$$

In these expressions, the adiabatic Hamiltonian $\hat{\mathcal{H}}^A$, which describes the system with the scattering electron fixed at $\mathbf{r}_e$, is simply

$$\hat{\mathcal{H}}^A(\mathbf{r}_m;\mathbf{r}_e,R)=\hat{\mathcal{H}}_m^{(e)}(\mathbf{r}_m;R)+V_{em}(\mathbf{r}_m;\mathbf{r}_e,R)\ , \tag{4}$$

where $\hat{\mathcal{H}}_m^{(e)}$ is the electronic Hamiltonian of the molecule and V_{em} is the electron-molecule interaction potential energy[19]

$$V_{em}(\mathbf{r}_m;\mathbf{r}_e,R)=\sum_{i=1}^{N_e}\frac{1}{|\,\mathbf{r}_e-\mathbf{r}_i\,|}-\sum_{\alpha=1}^{N_n}\frac{Z_\alpha}{|\,\mathbf{r}_e-\mathbf{R}_\alpha\,|}\ . \tag{5}$$

In Eq. (5), N_e and N_n are the number of electrons and nuclei in the target, and Z_α is the charge of the nucleus located at $\mathbf{R}_\alpha$.

Asymptotically, the adiabatic polarization potential (for a $D_{\infty h}$ molecule) reduces to the simple analytic form

$$V_{\rm pol}^A(\mathbf{r}_e;R)\underset{r_e\to\infty}{\sim}-\frac{\alpha_0(R)}{2r_e^4}-\frac{\alpha_2(R)}{2r_e^4}P_2(\cos\theta_e)\ , \tag{6}$$

where $\alpha_0(R)$ and $\alpha_2(R)$ are the spherical and nonspherical components of the polarizability of the target at internuclear separation R. One can derive this asymptotic form from the second-order correction to the system energy, as determined via time-independent perturbation theory[20,21] by treating V_{em} as a small perturbation due to a stationary electron located in the asymptotic region.

By contrast with this perturbative viewpoint, our procedure—in which $V_{\rm pol}^A$ is determined as the difference (3) between two energy-optimized functionals—includes contributions from terms of higher-than-second order in the interaction potential V_{em}. Nearer the target, where V_{em} is comparatively

large, these higher-order corrections can become important.[22] Hence, we expect a variationally determined adiabatic polarization potential to be more accurate in this region than one obtained from second-order perturbation theory, although both potentials should reduce to (6) far from the target.

The adiabatic approximation is predicated on the assumption that the target electrons respond adiabatically to the motion of the scattering electron, i.e., that the molecular charge distribution adjusts immediately to changes in the instantaneous position of the projectile. This approximation is valid for slow (low-energy) collisions *except near the target,* where the static-exchange interaction is strongly attractive and the "local velocity" of the scattering electron becomes comparable to that of the bound electrons. So if the projectile is near the target, then the response of the molecular electrons is not adiabatic, and $V_{\rm pol}^{A}$ [Eq. (3)] overestimates the true effects of polarization.

Within this picture, one can identify three "regions" of the polarization interaction depending on the distance of the scattering electron from the target. In the outermost (asymptotic) region, second-order perturbation theory is valid, and the polarization interaction is given by the limit (6). For the second (intermediate) region, the adiabatic approximation is valid, but contributions from terms of higher-than-second order in V_{em} should be included in $V_{\rm pol}^{A}$. Finally, in the near-target region, $V_{\rm pol}^{A}$ overestimates polarization effects, and nonadiabatic corrections must be taken into account.

One can use a variety of strategies to deal with these nonadiabatic effects. A particularly simple (though crude) method is a semiempirical approach based on the known asymptotic form (6). In this *phenomenological polarization potential,* short-range nonadiabatic effects are mimicked by multiplying Eq. (6) by a spherical cutoff function $C(r_e)$, viz.,

$$V_{\rm pol}^{\rm phen}(\mathbf{r}_e;R)=C(r_e)\left[-\frac{\alpha_0(R)}{2r_e^4}-\frac{\alpha_2(R)}{r_e^4}P_2(\cos\theta_e)\right] . \tag{7}$$

The spherical cutoff function is usually represented as

$$C(r_e)=1-\exp[-(r_e/r_c)^p] , \tag{8}$$

where p and r_c are adjustable parameters. For electron-molecule collisions the power parameter p is usually chosen as $p=6$, and the cutoff radius r_e is usually "tuned" (see examples in Ref. 3) to bring calculated cross sections into agreement with an experimentally determined feature of the scattering, such as a shape resonance. The cutoff function (8) approximates nonadiabatic effects in an *ad hoc* fashion by smoothly removing the polarization interaction when $r_e \le r_c$. Prior studies of polarization potentials, however, have shown that for some systems, the adiabatic potential $V_{\rm pol}^{A}$ deviates significantly from Eq. (7) in the intermediate region, where the adiabatic approximation is accurate.[22,23]

By contrast, we include nonadiabatic effects via a nonpenetrating approximation. Essentially, this approximation amounts to "turning off" the Coulomb interaction between the projectile and the bound electrons whenever the former is inside the charge cloud of the latter. This gambit yields a polarization potential that is free of adjustable parameters. The idea of using such an approximation to incorporate nonadiabatic effects originated in the polarized-orbital (PO) theory of electron-atom scattering.[12] Hence it is important to emphasize that *our polarization potential is not based on a PO treatment.* Our realization of this approximation for the structurally simpler e-H_2 system is described in detail in Ref. 11; here we shall merely sketch the basic idea.

To implement the nonpenetrating approximation, we modified the POLYATOM molecular structure code,[24] which we use to evaluate the perturbed and unperturbed energies (1) and (2), by altering the subroutines that calculate matrix elements of the aforementioned Coulomb interaction $|\mathbf{r}-\mathbf{r}_e|$ between two basis functions. In these subroutines, we multiply the adiabatic Hamiltonian (4) by a step-function cutoff that "switches off" this interaction for target charge density outside the radial position of the projectile, r_e.

When the bound-free Coulomb potential is subjected to the usual multipole expansion, the (nonpenetrating) matrix element of this potential between two basis functions becomes a sum over terms identified by the Legendre polynomial $P_\lambda(\cos\theta)$, where θ is the angle between $\mathbf{r}$ and $\mathbf{r}_e$ [see Eqs. (21)–(24) of Ref. 11]. Consistent with our earlier implementation of the variationally determined nonpenetrating polarization theory, we have retained only the dipole ($\lambda=1$) term in this sum. This simplification leads to the present "better-than-adiabatic dipole" polarization potential.

Thus we replace the standard multipole expansion of $1/|\mathbf{r}-\mathbf{r}_e|$ by the cutoff dipole form

$$\frac{1}{|\mathbf{r}-\mathbf{r}_e|}=\begin{cases}\dfrac{r}{r_e^2}\cos\theta_e, & r\le r_e\\ 0, & r>r_e ,\end{cases} \tag{9}$$

where $\mathbf{r}$ is the coordinate of a bound electron. To complete the evaluation of the matrix element of this potential between (Cartesian Gaussian) basis functions $\eta_s(\mathbf{r})$ and $\eta_t(\mathbf{r})$, we expand each in spherical harmonics, e.g.,

$$\eta_s(\mathbf{r})=\frac{1}{r}\sum_{l,m} a_{lm}^{s}(r)Y_l^m(\hat{\mathbf{r}}) , \tag{10}$$

and reduce the integration over $\mathbf{r}$ in the matrix element to a sum of angular terms and radial quadratures. Since the electronic configuration of N_2 includes occupied σ_g, σ_u, and π_u orbitals, we must evaluate the expansion coefficients in Eq. (10) for s-, p-, and d-type Cartesian Gaussian functions. Evaluating these integrals analytically and generalizing our computer programs to accommodate the increased range of orbitals and basis functions were the major steps in extending this method to molecules such as nitrogen.

In Sec. IV we shall compare our BTAD polarization potential and scattering quantities calculated with it to those determined by Onda and Temkin[10] using a PO po-

tential. Because the PO method is quite similar in some respects to our approach, it is worth briefly adumbrating the differences between the two strategies. Like the present approach, the PO method is based on the adiabatic approximation, retains only the dipole term in the expansion of the bound-free Coulomb potential, and accounts for nonadiabatic effects via the nonpentrating approximation. Unlike the present approach, the PO method further implements first-order perturbation theory to solve for the polarized orbitals and, in the application of Onda and Temkin,[10] replaces the exchange terms in the equations for these orbitals by a local free-electron-gas model exchange potential[25–28] that is scaled at each R for each orbital so as to bring the induced moments $\alpha_0(R)$ and $\alpha_2(R)$ into agreement with results of other calculations (see Table III of Ref. 10).

Onda and Temkin[10] used their PO potential to calculate vibrational excitation e-N_2 cross sections by solving two-dimensional fixed-nuclei (FN) scattering equations—replacing the nonlocal exchange terms by a scaled free-electron-gas model potential—using their noniterative partial-differential-equations (PDE) method.[29] Subsequently, Weatherford *et al.*[30] extended the PDE method in the FN approximation to incorporate exchange terms exactly, eliminating the need for a model exchange potential. In their scattering calculations (at $R=2.068a_0$), these authors altered the PO potential of Onda and Temkin,[10] multiplying it by a cutoff function of the form (8) with the power parameter $p=2$, and chose the adjustable cutoff radius r_c to position the $^2\Pi_g$ shape resonance at 2.39 eV, a value consistent with previous studies.[15,26,31] In Sec. IV A, we shall compare the PO potential, which we shall denote $V_{\rm pol}^{\rm (PO)}$, to the present variationally determined, parameter-free BTAD model.

B. Scattering theory

In Sec. IV we report integrated, differential, and rotational excitation cross sections for low-energy e-N_2 scattering. To facilitate comparison with results from other theoretical studies—and as the first step towards calculations that include vibrational effects—we evaluate these cross sections in the rigid-rotator approximation, fixing the internuclear separation of N_2 at $R=2.068a_0$.

The scattering calculations are based on the body-frame (BF) fixed-nuclei (FN) formulation of electron-molecule collision theory[32] (see Refs. 3 and 18 and references therein). In this formulation, coupled radial integro-differential scattering equations, expressed in single-center coordinates, are solved for a FN scattering function, the asymptotic behavior of which yields FN T matrices. From these matrices we determine total integrated cross sections and, via the adiabatic nuclear rotation (ANR) approximation,[32–35] rotational excitation cross sections. In the remainder of this section we will summarize the salient equations of this theory, identifying along the way critical convergence parameters of the calculation.

In the BF-FN formulation, the radial scattering equations separate according to electron-molecule symmetry; for a homonuclear target, each symmetry is identified by the behavior of the scattering function under inversion of the projectile coordinate (as gerade or ungerade) and by the absolute value of the projection of the projectile's orbital angular momentum along the internuclear axis, Λ. Adopting the notation of Sec. III of Ref. 18, we write the expansion in an angular basis (of partial waves) of the BF-FN scattering function for a given symmetry for a body energy $E_b=k_b^2$ (in rydbergs) as

$$ {}^{\rm FN}\Psi^{\Lambda}_{E_b,l_0}(\mathbf{r}_e;R)=\frac{1}{r_e}\sum_{l}^{l_{\max}} {}^{\rm FN}u^{\Lambda}_{l,l_0}(r_e;R)Y_l^{\Lambda}(\hat{\mathbf{r}}_e)\ . \tag{11}$$

By substituting this expansion into the Schrödinger equation for the projectile in the field of the ground (electronic) target state and projecting out an individual partial wave, one can derive the coupled radial scattering equations

$$\begin{aligned}\left[\frac{d^2}{dr_e^2}-\frac{l(l+1)}{r_e^2}-k_b^2\right]{}^{\rm FN}u^{\Lambda}_{l,l_0}(r_e;R)&\\ =2\sum_{l'}^{l_{\max}}V^{\Lambda}_{l,l'}(r_e)\,{}^{\rm FN}u^{\Lambda}_{l',l_0}(r_e;R)&\\ +2\sum_{l''}^{l^{\rm ex}_{\max}}\int K^{\Lambda}_{l,l''}(r_e,r_e')\,{}^{\rm FN}u^{\Lambda}_{l'',l_0}(r_e';R)dr_e'\ .&\end{aligned} \tag{12}$$

On the right-hand side of these equations one finds direct and exchange matrix elements. The former are expressed in terms of the Legendre projections v_λ of the direct potential—which includes the static and polarization components $V_{\rm st}$ and $V_{\rm pol}$—in the expansion[36]

$$V_{\rm st}(\mathbf{r}_e)+V_{\rm pol}(\mathbf{r}_e;R)=\sum_{\lambda}^{\lambda_{\max}}v_\lambda(r_e)P_\lambda(\cos\theta_e)\ . \tag{13}$$

Thus, the direct matrix elements are

$$\begin{aligned}V^{\Lambda}_{l,l'}(r_e)=\left[\frac{2l'+1}{2l+1}\right]^{1/2}\sum_{\lambda=0}^{\lambda_{\max}}v_\lambda(r_e;R)C(l'\lambda l;\Lambda 0)&\\ \times C(l'\lambda l;00)\ ,&\end{aligned} \tag{14}$$

where we have used the conventions of Rose[37,38] to write vector-coupling (Clebsch-Gordan) coefficients, such as $C(l'\lambda l;\Lambda 0)$.

We can express the other matrix elements in Eq. (12), the exchange matrix elements, in terms of the single-center expansion coefficients of the occupied molecular orbitals of the target. Letting ϕ^i_{l,Λ_i} denote the coefficient for the ith occupied orbital (with orbital angular momentum projection Λ_i), we write this expansion as

$$\phi_i^{\Lambda_i}(\mathbf{r}_e;R)=\frac{1}{r_e}\sum_{\bar{l}}^{l^{\rm MO}_{\max}}\phi^i_{\bar{l},\Lambda_i}(r_e;R)Y^{\Lambda_i}_{\bar{l}}(\hat{\mathbf{r}}_e)\ . \tag{15}$$

The resulting exchange matrix elements are written as a sum over the $N_{\rm occ}$ occupied orbitals, i.e.,

$$K^{\Lambda}_{l,l''}(r_e,r_e';R)=-\sum_{\lambda=0}^{\lambda_{\max}}\frac{r_<^{\lambda}}{r_>^{\lambda+1}}\sum_{\bar{l},\bar{l}'}^{l^{\mathrm{MO}}_{\max}}\sum_{i=1}^{N_{\mathrm{occ}}} g_{\lambda}(ll''\bar{l}\bar{l}';\Lambda\Lambda_i)\phi^{i}_{\bar{l},\Lambda_i}(r_e';R)\phi^{i}_{\bar{l}',\Lambda_i}(r_e';R)\ , \tag{16}$$

where $r_<=\overset{\max}{\min}\{r_e,r_e'\}$ and the constants g_λ are products of four vector coupling coefficients.[26]

To solve the scattering equations (12) numerically we adopt the linear algebraic method of Schneider and Collins.[5] In this method, the coupled FN scattering equations (11) are first recast as integral equations that incorporate the appropriate boundary conditions via a Green's function. These coupled integral equations are then transformed into a system of linear algebraic equations by imposing quadrature approximations on all integrals. The resulting numerical formulation is stable, efficient, ripe for vectorization on a supercomputer. Unlike many applications of this method, we do not use a separable representation of the exchange kernel;[39] rather, we treat exchange effects directly, via the expansion in Eq. (16).

In Eqs. (11)–(16) there appear four limits on various summations: $l_{\max}, l^{\mathrm{ex}}_{\max}$, $l^{\mathrm{MO}}_{\max}$, and $\lambda_{\max}$. Their presence results from our use of the close-coupling approximation to truncate the (in principle infinite) sums in the expansions (11), (13), and (15). Together with the maximum value $r_{\max}$ of the projectile coordinate r_e — the value at which the FN T-matrix elements ${}^{\mathrm{FN}}T^{\Lambda}_{l,l_0}(R)$ are extracted from the matrix of radial scattering functions that solve Eqs. (12)—these four limits constitute the "convergence parameters" of the present calculations. Their determination is the subject of Sec. III.

III. METHODOLOGICAL MINUTIAE

A. The N_2 target

The static and exchange terms and the BTAD polarization potential are all based on a near-Hartree-Fock (HF) representation of the occupied molecular orbitals of the $X\,{}^1\Sigma_g^+$ (ground) electronic state of N_2. To represent this state, we used a basis of contracted nucleus-centered Cartesian Gaussian functions that was determined by Morrison and Hay[22] in their study of the R dependence of the polarizability of N_2. This basis, which describes the unpolarized neutral target, is a $(9s5p1d/5s3p1d)$ contraction of a $(9s5p)$ nitrogen basis[40] with an additional $3d$ function to facilitate bond formation.[41]

In calculating the BTAD potential, we must augment this basis to make it sufficiently flexible that it can represent distortions of the target charge density by the (fixed) scattering electron. To this end, we added to this neutral basis uncontracted, s, p, and d functions,[22] resulting in a $(6s4p2d)$ basis. For an internuclear separation $R=2.068a_0$, this basis yields a ground-state HF energy[42] of $-108.9746E_h$. By contrast, the (essentially exact) partial-wave HF electronic energy for this internuclear separation is[43] $-108.9928E_h$.

The unpolarized ground-state HF electronic wave function [from the $(6s5p2d)$ basis] is used to calculate the static potential[36] V_{st} in Eq. (13). In the limit $r_e\to\infty$, the Legendre projections of this potential define the permanent multipole moments of the molecule as

$$v^{\mathrm{st}}_{\lambda}(r_e;R)=\frac{2\lambda+1}{2}\int_0^{\pi}V_{\mathrm{st}}(\mathbf{r}_e;R)P_{\lambda}(\cos\theta_e)\sin\theta_e\,d\theta_e \underset{r_e\to\infty}{\sim}-\frac{c_{\lambda}(R)}{2r_e^{\lambda+1}}\ . \tag{17}$$

For our (augmented) neutral $X\,{}^1\Sigma_g^+$ basis, the first three moments for $R=2.068a_0$ are[44,45]

$$\begin{aligned} c_2(R)&=-0.91ea_0^2\ ,\\ c_4(R)&=-7.41ea_0^4\ ,\\ c_6(R)&=-20.68ea_0^6\ . \end{aligned} \tag{18}$$

These values were extracted from the Legendre projections in (17) at $r_e=10.0a_0$, by which point each projection $v^{\mathrm{st}}_{\lambda}(r_e;R)$ had settled down to its limiting multipole form [to the precision shown in Eqs. (18)]. For comparison, the experimental value, as determined from measurements of induced birefringence, of the average of this moment over the ground vibrational state of N_2 is[46,47] $c_2=-(1.04\pm0.07)ea_0^2$.

Similarly, we can extract the (fixed-R) polarizabilities of the target from the asymptotic limit of the first two Legendre projections of the BTAD polarization potential [see Eq. (7)]. For $R=2.068a_0$ we obtain from these projections at $r_e=25a_0$ the values

$$\begin{aligned} \alpha_0(R)&=11.42a_0^3\ ,\\ \alpha_2(R)&=3.37a_0^3\ . \end{aligned} \tag{19}$$

The static spherical polarizability was measured by Newell and Baird[48] and by Orcutt and Cole[49] to be $\alpha_0=(11.744\pm0.004)a_0^3$ at room temperature (i.e., averaged over the ground electronic state). Bridge and Buckingham[47,50] measured the relative polarizability anisotropy α_2/α_0 at 633 nm; this ratio is likely to be the same at zero frequency, implying that $\alpha_2=(3.08\pm0.002)a_0^3$.

B. Three polarization potentials

At various stages of the present investigation of e-N_2 scattering we used three polarization potentials. Foremost among these is the BTAD potential, which, as described in Sec. II A, is free of adjustable parameters and allows for nonadiabatic effects via the nonpenetrating approximation of Eq. (9). We also calculated selected cross sections using the correlation-polarization (CP) potential of O'Connell and Lane,[14] which Padial and Norcross have also applied to this system,[15] and the phenomenological potential (7), using values of the power and cutoff parameters from an earlier study by Morrison and Collins.[26] Here we shall briefly describe salient computational features of these potentials.

1. The BTAD potential and its two-term approximation

In our initial verifications of our computer programs, we considered a *purely adiabatic* e-N_2 potential $V_{\rm pol}^{\rm AD}$ so as to allow comparison at the level of the potential with prior results.[22,23] We calculated this potential variationally (see Sec. II A) without invoking the nonpenetrating approximation. In spite of differences in the basis sets used in these three studies, the polarization potentials agree well. For example, for the electron fixed at $x_e=2.0a_0$, Morrison and Hay[22] report a polarization potential of $-0.094E_h$, Eades *et al.*[23] report $-0.095E_h$, and the present calculations produce $-0.104E_h$; for $z_e=2.0a_0$, these values are $-0.494E_h$, $-0.473E_h$, and $-0.490E_h$, respectively. The parallel and perpendicular polarizabilities, as extracted from the large-r_e values of the potential, show comparable agreement.

Another point about the present realization of the BTAD potential requires comment. We represent this potential by a *two-term* Legendre expansion—i.e., we retain only the $\lambda=0$ and $\lambda=2$ coefficients *of the polarizations potential* in the expansion (13) of the direct potential. (Of course, far more than two terms in the expansion of the static potential must be retained.) The accuracy of this approximation is discussed by Morrison and Hay,[22] who show that for a purely adiabatic potential, under certain circumstances, higher-order contributions to $V_{\rm pol}$ may be important.

To check the two-term approximation for the BTAD potential, we performed self-consistent-field calculations (using the POLYATOM molecular structure package) of the *full* polarization potential $V_{\rm pol}^{\rm BTAD}(r_e,\theta_e;R)$ at several radial positions r_e for five projectile angles: $\theta_e=0$ (on the z axis), 18.36°, 42.14°, 66.06°, and 90.0° (on the x axis). These self-consistent-field (SCF) values were than compared to their two-term approximates, $v_0^{\rm pol}(r_e;R)+v_2^{\rm pol}(r_e;R)\,P_2(\cos\theta_e)$.

For all values of r_e sampled, we found the two-term approximation *to the BTAD potential* to be accurate to better than 1%. Interestingly, this level of agreement is not obtained for a purely adiabatic potential. For example, at $r_e=1.5a_0$, the two-term and SCF adiabatic potentials disagree by 3% at all angles; nearer to the target, the errors introduced by the two-term approximation for the adiabatic potential are quite large, while those for the BTAD potential remain small. Thus, the (approximate) inclusion of nonadiabatic effects in the BTAD potential mitigates the error noted by Morrison and Hay[22] due to the two-term approximation.

2. The correlation-polarization potential

The CP potential is determined by "hooking" a short-range model correlation potential to the asymptotic form of the polarization potential, Eq. (7). The correlation potential, which is a parameter-free model based on the application of the local density approximation to the free-electron-gas model of the target, can easily be calculated from the undistorted probability density of the target molecule.

In a variety of applications in the rigid-rotator approximation[15,16] the CP potential has yielded cross sections that agree remarkably well with experimental data (where such comparison are possible). A recent study of this model potential for vibrational excitation of H_2, however, raised questions about its accuracy for this scattering process.[51]

In any case, the present study affords an opportunity to compare the CP and BTAD models in the carefully controlled context of scattering calculations based on identical occupied orbitals, using identical numerical procedures and computer programs, and in which identical, stringent convergence criteria could be (and were) imposed.

As in our realization of the BTAD potential, only the $\lambda=0$ and 2 Legendre projections in the single-center expansion of the CP potential are retained. Examination of the analytic form for this potential [see Eq. (9) of Ref. 15] shows that these projections are fully described by four R-dependent parameters: the radius $r_c^\lambda(R)$ at which each component of the (short-range) correlation potential crosses (and hence is joined to) the asymptotic polarization term $-\alpha_\lambda(R)/2r_e^4$, and the value of $v_\lambda^{\rm CP}$ of the λ projection of the CP potential at this radius.

We calculated the CP potential using (in the correlation part) the ground-state N_2 basis described in Sec. III A. The resulting parameters are compared to those of Padial and Norcross[15,52] in Table I.

3. The semiempirical heuristic polarization potential

Finally, we performed a few scattering calculations using a phenomenological polarization potential (7). In a prior study of e-N_2 scattering, Morrison and Collins[26] used such a form together with a near-Hartree-Fock static potential, which they calculated from the ground-state electronic function of Cade *et al.*,[45] and a tuned free-electron-gas model exchange potential. Although their cross sections agreed rather well with existing ex-

TABLE I. Parameters of the correlation-polarization potential for N_2 (see Ref. 52).

	r_c^0 (units of a_0)	r_c^2 (units of a_0)	$-v_0^{\rm CP}(r_c^0;R)$ (units of E_h)	$-v_2^{\rm CP}(r_c^2;R)$ (units of E_h)
Present[a]	3.625	3.825	0.033 07	0.007 87
Padial and Norcross[b] (Ref. 15)	3.5	3.4	0.0379	0.011

[a]Based on Eq. (9) of Ref. 15.
[b]Based on Eq. (6) of Ref. 15.

perimental data, the validity of their phenomenological polarization potential was hard to assess because a model exchange potential was also used in this study—which feature made it impossible to determine the extent to which inaccuracies in one model potential might be compensating for weaknesses in the other.

In order to shed some light on this matter and on the validity of these widely used heuristic forms, we carried out new scattering calculations with this potential using the parameters determined by Morrison and Collins.[26] That is, rather than retune the cutoff function (8), we simply adopted their values of $p=6$ for the power parameter and $r_c=2.341a_0$ for the cutoff radius. The latter value was chosen to position the $^2\Pi_g$ shape resonance in their model-exchange cross section at the experimentally determined energy[53] of 2.39 eV.

C. Parameters of the scattering calculations

We converged the scattering quantities (cross sections and eigenphase sums) reported in Sec. IV to 1% at energies up to 1.0 Ry in the six "lowest" electron-molecule (BF-FN) symmetries: Σ_g, Σ_u, Π_g, Π_u, Δ_g, and Δ_u. Differential cross sections, which are more sensitive, were converged separately to this accuracy. To ensure convergence, the following four quantities must be determined.

$l_{\max}$, the maximum order partial wave (spherical harmonic, with z as the quantization axis) included in the expansion (11) of the BF-FN scattering function.

$l_{\max}^{\text{ex}}$, the maximum order partial wave included in the expansion of the scattering function *in the exchange term* in the coupled equations (12).

$l_{\max}^{\text{MO}}$, the maximum order partial wave included in the expansion (15) of the occupied (bound) molecular orbitals in the exchange kernel (16).

$r_{\max}$, the radius at which the BF-FN scattering matrix is extracted from the solution matrix.

The last of these parameters calls for further comment. We used the linear algebraic method *per se* only for $r_e<6.0a_0$; outside a sphere of this radius, the interaction potential reduces to a smoothly dying asymptotic form [see Eqs. (7) and (17)], and it is (far) more efficient to call upon a standard propagative scheme to get to $r_{\max}$. To this end, we use the R-matrix propagator method as implemented by Light and Walker.[54] We can check that our maximum radius is large enough to accommodate all significant distortion of the scattering function by the simple expedient of integrating the coupled equations still farther. As exemplified by the data at $E_b=0.1$ Ry in Table II, integrating these equations for the Σ_g, Σ_u, Π_g, Π_u, Δ_g, and Δ_u symmetries to $r=100a_0$ confirms that $r_{\max}=85.0a_0$ is sufficient to converge our cross sections to the desired accuracy. Similar tests at (body) scattering energies of 0.5 and 1.0 Ry established that this maximum radius is appropriate to the entire energy range considered in this work.

In the region where the linear algebraic method *is* used, we exploited one of its most useful features: the ability to use different (radial) quadrature meshes for different channels.[55] This feature enabled us to optimize time and accuracy. After extensive convergence studies in which we varied the number of points in various channel ranges, we determined our final (Gauss-Legendre) quadrature mesh. It consists of 50 points for the first six channels in the Σ, Π, and Δ symmetries: 10 points from 0.0 to 0.7, 24 points from 0.7 to 1.5, 10 points from 1.5 to 2.5, and 6 points from 2.5 to 6.0. For the remaining channels, we use 6 points from 0.0 to 0.7, 14 points from 0.7 to 1.5, and 6 points from 1.5 to 6.0.

We now turn to the various quantities that control the upper limits on expansions in the formalism in Sec. II B. In order to determine the number of continuum partial waves one must include in the coupled scattering equations, we began with the number of channels in the direct and exchange terms equal; i.e., with $l_{\max}=l_{\max}^{\text{ex}}$.

TABLE II. Convergence studies for e-N_2 scattering in the static-exchange approximation (see Sec. IV B): Σ_g eigenphase sums and partial cross sections at $E_b=0.01$ Ry. The convergence parameters are described in Sec. II B. For each test, only those convergence parameters that are changed are listed on all three lines; in each case, the **bold-faced** value of each parameter is the one used in the calculations that produced the results of Sec. IV.

$l_{\max}$	$l_{\max}^{\text{ex}}$	$l_{\max}^{\text{MO}}$	$r_{\max}$	$\delta(\Sigma_g)$	$\sigma(\Sigma_g)$
22	10	6	50.0	2.4004	55.4152
			85.0	2.4002	55.4122
			100.0	2.4002	55.4116
22	4	4	85.0	2.8917	73.4865
		10		2.8933	72.5980
		16		2.8932	72.6000
22	4	16	85.0	2.8932	72.5000
	12			2.9007	68.3050
	16			2.9008	68.2377
14	14	4	85.0	2.3541	61.2069
22	22			2.3752	58.5773
28	28			2.3794	58.6032

Subsequently, we could reduce the number of continuum partial waves included in the exchange term, resulting in a considerable savings of computer time with no attendant loss of accuracy. Examples of the convergence properties of the eigenphase sums and partial cross sections in the (particularly sensitive) Σ_g symmetry at $E_b=0.01$ Ry are shown in Table II. *Note that these studies were performed in the static-exchange approximation (see Sec. IV B) to facilitate comparison of our results to those of other investigators.* We performed similar convergence tests at the additional test energies 0.5 and 1.0 Ry, which span the energy range considered in this study.

Especial care is required in treating the molecular orbital expansion in the exchange kernel—for in a calculation in which exchange effects are treated exactly, each additional such term results in a large increase in computer time. As Table II illustrates, we could obtain the desired 1% accuracy by including 10 terms in this expansion, a limit we checked via scattering calculations including 16 such terms at the aforementioned test energies. For energies near 1.0 Ry and in symmetries other than Σ_g, one can use one or two fewer terms in this expansion with no loss of accuracy.

IV. RESULTS AND INTERPRETATION

A. Polarization potentials

Consistent with the two-term approximation discussed in Sec. III B 1, we calculated the $\lambda=0$ and 2 Legendre projections of the purely adiabatic and the BTAD polarization potentials from their SCF values $V_{\rm pol}(r_e,\theta_e;R)$ [see, for example, Eq. (3) for the adiabatic potential], positioning the projectile on the BF z axis ($\theta_e=0$) and on the x axis ($\theta_e=\pi/2$):

$$v_0^{\rm pol}(r_e;R)=\tfrac{1}{3}[2V_{\rm pol}(r_e,\pi/2;R)+V_{\rm pol}(r_e,0;R)]\ , \qquad (20a)$$

$$v_2^{\rm pol}(r_e;R)=\tfrac{2}{3}[V_{\rm pol}(r_e,\pi/2;R)-V_{\rm pol}(r_e,0;R)]\ . \qquad (20b)$$

In Figs. 1, these projections are graphed together with those of the CP potential of Sec. III B 2 and of the PO potentials of Onda and Temkin[10] and of Weatherford *et al.*[30]

Several points of interest are apparent in these figures. First, in the near-target region, the BTAD and CP potentials are noticeably weaker than the purely adiabatic form. This weakening of polarization potentials at small r_e is a manifestation of higher-order nonadiabatic terms, which these two models approximate; this effect has been studied in depth for the e-He system.[56]

Second, the PO potentials differ from the others discussed in this section in one important respect: They are repulsive along the x axis for small r_e. This feature causes the spherical projection of the PO potential to be positive for $r_e<0.5a_0$, unlike the BTAD or CP (or purely adiabatic) potentials. We also note that the $\lambda=2$ projection of the PO potential of Onda and Temkin[10] is considerably stronger for $r<1.5a_0$ than any of the other potentials considered here, including the purely adiabatic form—a result that is somewhat surprising, since

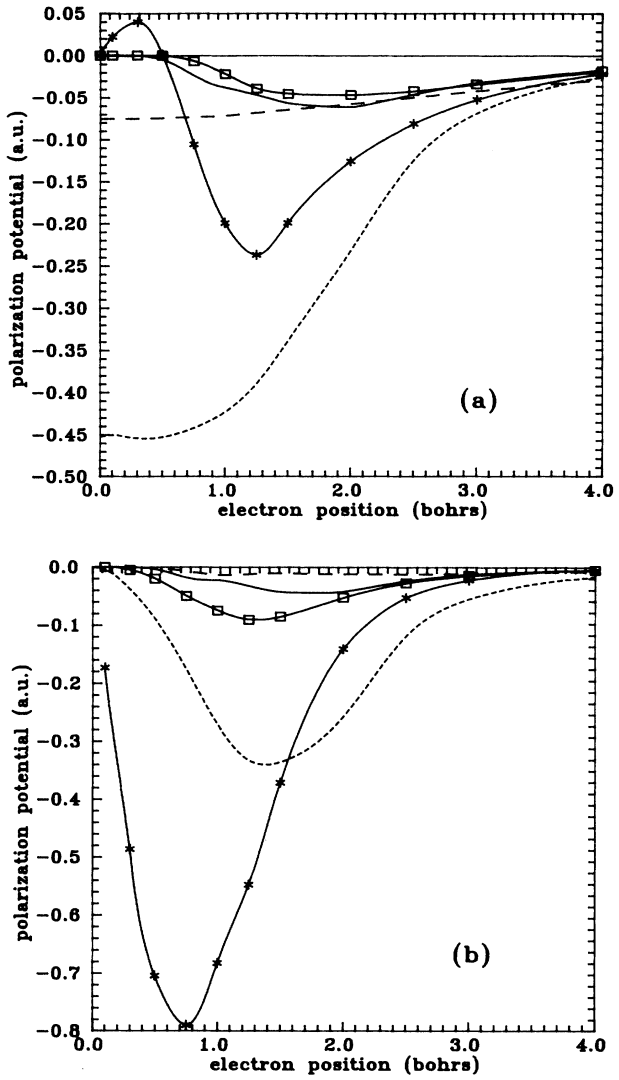

FIG. 1. (a) Spherical ($\lambda=0$) and (b) nonspherical ($\lambda=2$) projections of e-N_2 polarization potentials at $R=2.068a_0$. The BTAD (solid curve) and CP (long-dash curve) potentials are described in Sec. II as is the purely adiabatic potential (short-dash curve). Also shown are the polarized orbital potential of Onda and Temkin (Ref. 10) (solid curve with stars) and the cutoff form of this potential used by Weatherford *et al.* (Ref. 30) (solid curve with squares).

Onda and Temkin implemented the same nonpenetrating approximation in their PO calculations as we did in generating our BTAD model. In any case, the cutoff function [Eq. (8) with $p=2$] used by Weatherford *et al.*[30] ameliorates this difference, bringing both projections of the PO potential into closer agreement with the other two nonadiabatic models.

The $\lambda=0$ and 2 components of our BTAD potential are tabulated in Table III; sufficient points are given in this table so that, if desired, both projections can be accurately interpolated (via, say, a cubic-spline interpola-

tor) onto the integration mesh of a future scattering calculation. For greater ease of implementation, we have also fitted this potential to a convenient analytic form

$$v_\lambda^{\mathrm{BTAD}}(r_e;R)=-D\frac{1-e^{-(r_e/r_0)^f}}{(ar_e^2+br_e+c^2)^2} . \tag{21a}$$

Note that none of the constants in this form—including the constant r_0—was determined by recourse to experimental data; instead, all were obtained from the fit to the numerical potential in Table III. The values of these constants are

$$\text{For } \lambda=0 \begin{cases} a=0.97, \quad b=-1.66, \quad c=2.83 \\ D=4.7, \quad r_0=1.35, \quad f=2.62, \quad 0\le r_e\le 6.0a_0 \\ a=0.98, \quad b=0, \quad c=0.95 \\ D=5.7, \quad r_0=1.35, \quad f=2.62 , \\ \qquad\qquad 6.0\le r_e\le 25.0a_0 , \end{cases} \tag{21b}$$

$$\text{For } \lambda=2 \begin{cases} a=1.6, \quad b=0.16, \quad c=1.9 \\ D=4.75, \quad r_0=1.59, \quad f=4.7, \quad 0\le r_e\le 8.0a_0 \\ a=1.0, \quad b=0, \quad c=0 \\ D=1.68, \quad r_0=1.59, \quad f=4.7 , \\ \qquad\qquad 8.0\le r_e\le 25.0a_0 . \end{cases} \tag{21c}$$

TABLE III. Legendre projections of the BTAD polarization potential at $R=2.068a_0$ for $\lambda=0$ and $\lambda=2$ [see Eqs. (20)]. The values of the projections are given in atomic units (hartrees). A fit to these data appears in Eqs. (21). (Note: $1.0[-04]=1.0\times10^{-4}$.)

r_e (units of a_0)	$v_0^{\mathrm{BTAD}}(r_e;R)$	$v_2^{\mathrm{BTAD}}(r_e;R)$
0.10	−0.5732[−06]	−0.4317[−06]
0.20	−0.3405[−04]	−0.2621[−04]
0.50	−0.4958[−02]	−0.4059[−02]
0.75	−0.2386[−01]	−0.1847[−01]
0.90	−0.3454[−01]	−0.2312[−01]
1.00	−0.3831[−01]	−0.2290[−01]
1.15	−0.4372[−01]	−0.2796[−01]
1.25	−0.4739[−01]	−0.3308[−01]
1.50	−0.5711[−01]	−0.4357[−01]
2.00	−0.6130[−01]	−0.4162[−01]
2.50	−0.4593[−01]	−0.2336[−01]
3.00	−0.3199[−01]	−0.1194[−01]
4.00	−0.1677[−01]	−0.4705[−02]
5.00	−0.8499[−02]	−0.2414[−02]
6.00	−0.4341[−02]	−0.1272[−02]
7.00	−0.2373[−02]	−0.7011[−03]
8.00	−0.1395[−02]	−0.4127[−03]
9.00	−0.8715[−03]	−0.2579[−03]
10.00	−0.5717[−03]	−0.1692[−03]
15.00	−0.1129[−03]	−0.3339[−04]
20.00	−0.3572[−04]	−0.1057[−04]
25.00	−0.1462[−04]	−0.4308[−05]

B. Scattering in the static-exchange approximation

Although physically unrealistic, the static-exchange (SE) approximation—in which one neglects polarization and correlation effects—is important to theorists, for it is the foundation on which they erect investigations (such as the present one) of polarization.[3,4] A foundation of accurate SE calculations is particularly important for comparisons of scattering quantities based on different treatments of polarization; unless the static and exchange interactions are unerringly included, such comparisons are of dubious significance. This explains the extensive attention theorists have paid over the years to e-N_2 scattering in this approximation.[57–59]

We have calculated BF-FN eigenphase sums and cross sections in the SE approximation in the Σ, Π, and Δ e-N_2 symmetries at five selected energies—first, to check our linear algebraic code, and second, to compare our treatment of SE effects with those adopted in prior research on this system. In these calculations, we included the direct nonlocal exchange kernel (16), rather than apply the widely used separable representation of this kernel.[39] As a cross check, we calculated scattering quantities using a wholly different computer program based on the iterative static-exchange method of Collins *et al.*;[59] the two codes gave results identical to within the convergence criterion (1%) imposed on both calculations.

The scattering quantity that at low, nonresonant energies is most sensitive to exchange is the eigenphase sum in the Σ_g symmetry. In Table IV we compare our values for this quantity at three energies with those of other SE studies. The results in this table are split into two classes, depending on whether exchange was treated directly or via a separable representation on a finite basis. Included in this table are the present exact-exchange, linear-algebraic calculations and those of Collins,[60] which were based on the $X\,^1\Sigma_g$ N_2 wave function of Cade *et al.*[45] To suggest the accuracy of the separable approximation, we also show separable-exchange, linear-algebraic eigenphase sums calculated by Collins.[60]

TABLE IV. Electron-N_2 eigenphase sums in the Σ_g symmetry at $R=2.068a_0$ in the static-exchange approximation.

Energy (Ry)	0.10	0.50	1.00
	Exact exchange		
Present	2.4067	1.7386	1.3135
Linear algebraic[a]	2.4096	1.7398	1.3107
R matrix[b]	2.433	1.771	1.229
PDE method[c]	2.417	1.747	1.350
	Separable exchange		
Linear algebraic[a]	2.423	1.730	1.342
T matrix[d]	2.425	1.726	1.295

[a]Collins, Ref. 60.
[b]Burke *et al.*, Ref. 6.
[c]Weatherford *et al.*, Ref. 30.
[d]Meyer, Ref. 58.

TABLE V. Electron-N_2 static-exchange eigenphase sums and partial cross sections in all Σ, Π, and Δ symmetries at $R = 2.068a_0$. For each energy, the top line gives the eigenphase sum (in radians) and the lower line gives the corresponding cross section (in square bohr) in parentheses.

E (Ry)	Σ_g	Σ_u	Π_u	Π_g	Δ_g	Δ_u
0.10	2.4067	2.9711	3.0698	0.0141	0.0137	3.1390
	(54.624)	(3.230)	(1.046)	(0.104)	(0.076)	(0.0016)
0.25	2.0542	2.7437	2.9169	0.8170	0.0440	3.1394
	(39.000)	(7.065)	(4.546)	(54.330)	(0.245)	(0.0021)
0.50	1.7386	2.4454	2.7131	2.5279	0.1368	0.0069
	(24.423)	(10.249)	(8.604)	(16.126)	(1.023)	(0.0105)
0.75	1.5137	2.2379	2.5744	2.5281	0.2554	0.0281
	(16.755)	(10.966)	(10.515)	(10.751)	(2.218)	(0.0440)
1.00	1.3135	2.1131	2.4872	2.4908	0.3713	0.0601
	(12.347)	(10.641)	(11.301)	(9.051)	(3.314)	(0.1174)

TABLE VI. Electron-N_2 static-exchange-polarization eigenphase sums and partial cross sections in Σ and Π symmetries at $R = 2.068a_0$. For each energy, the top line gives the eigenphase sum (in radians) and the lower line gives the corresponding cross sections (in square bohr) in parentheses. Also shown on the second line for each energy are the total integrated and momentum transfer cross sections (*in square angstroms*); these results include contributions from Δ symmetries. (Only selected energies are shown; a complete table is available on request from the authors.)

E (Ry)	Σ_g	Σ_u	Π_u	Π_g	σ_{tot}	σ_{mom}
0.0007	3.1226	3.1396	3.1446	0.000		
	(6.145)	(0.070)	(0.323)	(0.000)	1.832	2.110
0.0015	3.1106	3.1383	3.1475	0.000		
	(8.029)	(0.093)	(0.633)	(0.001)	2.459	2.920
0.0029	3.0906	3.1378	3.1514	0.000		
	(10.669)	(0.065)	(0.906)	(0.005)	3.281	3.945
0.0051	3.0657	3.1378	3.1562	0.000		
	(13.578)	(0.035)	(1.149)	(0.01)	4.165	5.063
0.0100	3.0203	3.1384	3.1646	0.0007		
	(18.036)	(0.016)	(1.462)	(0.014)	5.508	6.730
0.0500	2.7927	3.1280	3.1929	0.0223		
	(31.101)	(0.065)	(1.207)	(0.252)	9.238	10.358
0.1000	2.6219	3.0831	3.1824	0.1103		
	(34.3878)	(0.5428)	(0.287)	(2.908)	10.856	10.888
0.1500	2.5011	3.0261	3.1541	0.6659		
	(34.282)	(1.385)	(0.036)	(63.087)	27.929	27.702
0.2000	2.4086	2.9660	3.1193	2.4897		
	(33.036)	(2.381)	(0.296)	(47.263)	23.600	20.780
0.2500	2.3333	2.9067	3.0828	2.7322		
	(31.368)	(3.399)	(0.851)	(16.784)	15.148	12.200
0.3500	2.2134	2.7952	3.0120	2.8023		
	(27.770)	(5.257)	(2.314)	(8.795)	13.077	9.915
0.5000	2.0662	2.6519	2.9200	2.7943		
	(22.888)	(7.354)	(4.530)	(6.790)	12.749	9.558
0.7500	1.8495	2.4803	2.8098	2.7512		
	(16.698)	(9.248)	(7.356)	(6.067)	12.709	9.581
1.0000	1.6447	2.3966	2.7466	2.7118		
	(12.609)	(10.037)	(9.132)	(5.810)	12.564	9.409

The separable approximation was used in the T-matrix calculations of Meyer[58] but in none of the other studies quoted. Thus, Noble *et al.*[57] implemented the R-matrix method using a representation of the exchange kernel on a basis of Slater-type orbitals. The results from Weatherford *et al.*[30] were obtained using the aforementioned PDE method.

This table illustrates the degree of unanimity that has been achieved thus far in studies based on widely disparate numerical methods for solving the e-N_2 scattering problem at the SE level. Our exact-exchange linear-algebraic eigenphase sums and partial cross sections for the Σ and Π symmetries are given in Table V.

C. Diverse cross sections

Including polarization effects (by whatever means) wreaks considerable changes on the FN eigenphase sums and cross sections—as a comparison of Table V, which contains our SE results, and Table VI, which contains our static-exchange-polarization BTAD results, will attest. The sensitivity of these scattering quantities to how one includes polarization is illustrated by the Σ_g partial cross sections in Fig. 2. In addition to the present BTAD and CP results, this rather busy figure contains cross sections from the linear algebraic calculations of Schneider and Collins[5] and the R-matrix calculations of Burke *et al.*,[6] both of which treat polarization via an optical potential, from the Schwinger multichannel calculations by Huo *et al.*,[7] which is a pseudostate technique,

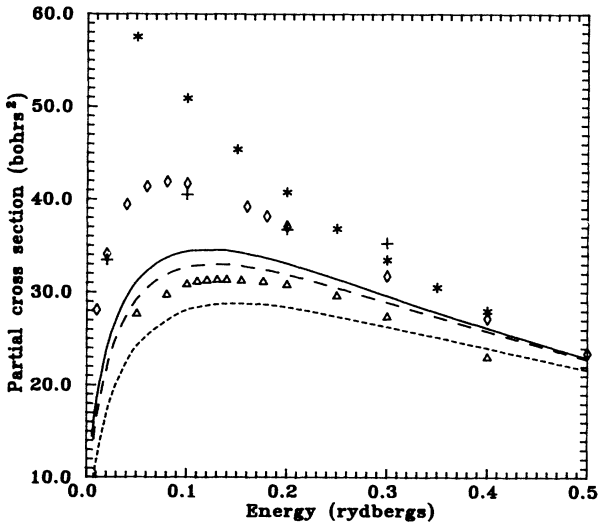

FIG. 2. Partial e-N_2 cross sections in the Σ_g symmetry. The BTAD (solid curve), CP (long-dash curve), and cutoff phenomenological (short-dash curve) results are from the present work. [The latter potential is based on Eq. (8) with parameters chosen from Ref. 26]. Also shown are results from model-exchange (with phenomenological polarization) calculations of Morrison and Collins (Ref. 26) (diamonds), the optical potential study of Schneider and Collins (Ref. 69) (pluses), the R-matrix study of Burke *et al.* (Ref. 6) (stars), and the Schwinger multichannel results of Huo *et al.* (Ref. 7) (triangles).

and from the close-coupling calculations of Morrison and Collins.[26]

In the latter calculation, polarization effects were approximated by the phenomenological model (7), using $p=6$ and $r_c=2.341a_0$ in the cutoff function, and exchange effects by a Hara free-electron-gas model exchange potential.[25] To explore the extent to which these two model potentials interacted in this earlier study, we calculated Σ_g cross sections using this polarization potential and parameters but treating exchange exactly. The results, shown by the dotted curve in Fig. 2, show that, as often happens when more than one model potential is used in a scattering calculation, the phenomenological polarization potential used by Morrison and Collins compensated for weaknesses in their model exchange potential. In fact, the shape resonance in the total integrated cross section, which Morrison and Collins positioned at 2.39 eV in the model-exchange calculation by tuning their polarization potential, occurs in the present exact-exchange calculation at 1.547 eV; the difference between these resonance energies is entirely attributable to the different treatment of exchange in the two studies.

1. Total and momentum transfer cross sections

The Σ_g cross sections in Fig. 2 are but one contributor to the total cross section, the sum of elastic and rotational excitation contributions. Our BTAD total cross sections—as calculated from FN scattering matrices in the Σ, Π, and Δ symmetries, augmented by contributions from higher symmetries in the first Born approximation—are compared to recent experimental data over the entire energy range considered in this study in Fig. 3(a). (An exhaustive survey of other measurements of e-N_2 cross sections appears in the review by Trajmar *et al.*[61])

Two experimental cross sections are featured in this figure. The absolute cross sections of Kennerly,[53] obtained with a transmission time-of-flight apparatus, encompass the full range of energies in the present theoretical study. Kennerly estimates his results to be accurate to $\pm 3\%$; below the resonance, these error bounds embrace our BTAD (and CP) results. The most recent measurement of total cross sections, by Suoeka and Mori,[62] is based on a retarding potential time-of-flight technique and produced cross sections at and above 1.2 eV. Poor resolution of the average energy perpendicular to the flight path of the electron caused the shape resonance peak obtained by Suoeka and Mori to lie below the generally accepted energy,[2,3,53] 2.4 eV.

Various theoretical cross sections, from this and other studies, at nonresonant energies are compared in Fig. 3(b). Like the theoretical studies that generated the Σ_g cross sections in Fig. 2, those in Fig. 3 include polarization via several different strategies. Particularly noteworthy in the latter figure is the close agreement of the BTAD and CP total cross sections.[63]

The most obvious difference between the theoretical total cross sections and the experimental results of Kennerly[53] is the lack in the former of oscillatory structure near the resonance. The use of the FN approxima-

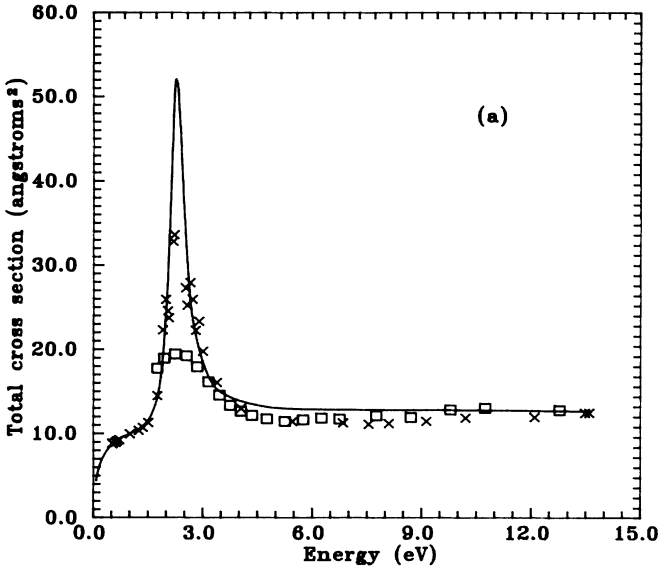

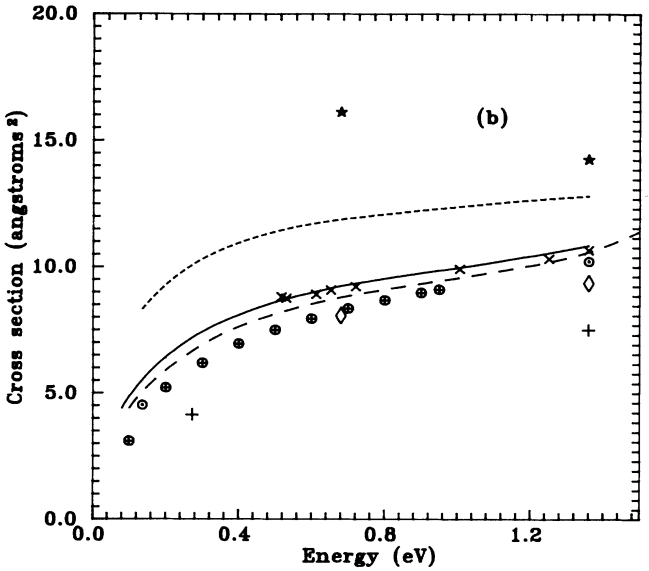

FIG. 3. Total integrated e-N_2 cross sections calculated with the BTAD potential (solid curve) compared to (a) experimental data of Kennerly (Ref. 53) (crosses) and of Suoeka and Mori (Ref. 62) (squares). (b) Theoretical total cross sections for the BTAD potential (solid curve), our CP potential (long-dash curve), and with the CP potential of Padial and Norcross (Ref. 15) (circles with dots). Also shown are the polarized orbital results of Weatherford *et al.* (Ref. 30) (circles with pluses), the Schwinger multichannel results of Huo *et al.* (Ref. 7) (diamonds), and the model-exchange (with phenomenological polarization) cross sections of Morrison and Collins (Ref. 26) (short-dash curve). Finally, we include the Σ_g integrated cross sections calculated using optical potential formulations by Burke *et al.* (Ref. 6) (stars) and by Schneider and Collins (Ref. 69) (pluses).

tion in our calculations precludes this structure—which does, however, appear if the dynamical interaction of the motions of the projectile and the nuclei are somehow taken into account, as in the work by Chandra and Temkin[64] using the hybrid theory; by Morgan[65] and by Schneider *et al.*[66] using the R-matrix method; by Dubé and Herzenberg[67] and by Hazi *et al.*[68] using the boomerang model; and by Berman and Domcke[31] using many-body optical-potential theory.

Nevertheless, our FN eigenphase sums in the $^2\Pi_g$ symmetry clearly exhibit a shape resonance (Table VI), and these data can be fitted to a Breit-Wigner form (modified to allow for background scattering) to yield the resonance energy E_r and width Γ for $R=2.068a_0$. These data are given in Table VII, where they are compared to results from several recent (parameter-free) studies. For comparison we use the experimental "reference values" determined by Berman *et al.*,[70] $E_r=2.32$ eV and $\Gamma=0.41$ eV. In all studies quoted in Table VII, the shape resonance appears at the indicated energy without adjustment or tuning in the calculation.

Direct measurement techniques yielded the total cross sections in Fig. 3(a); by contrast, indirect techniques—the numerical solution of the Boltzmann equation to analyze measured transport data—can be used to determine very-low-energy momentum transfer cross sections to high accuracy. In Fig. 4, our BTAD (total) momentum transfer cross sections are compared to the effective cross sections derived by Englehardt *et al.*[71] [Recently, Phelps and Pitchford[72] analyzed the validity of assumptions underlying these (and other) swarm-derived cross sections.]

2. *Elastic differential (and integrated) cross sections*

The most severe test of a theoretical calculation is to compare its differential cross sections to experiment.

TABLE VII. Energy and width of the $^2\Pi_g$ e-N_2 shape resonance as calculated using various methods of including polarization effects. [The eigenphase sums for the cutoff phenomenological potential (7) were calculated using the parameters p and r_c given in Morrison and Collins (Ref. 26); see Sec. IV C.]

Method	E_r (eV)	Γ (eV)
Present (BTAD)	2.253	0.472
Present (CP)	2.181	0.458
Present (phenomenological)	1.547	0.221
Integral equations[a] (CP)	2.17	0.47
Optical potential[b]	2.07	0.301
Stieltjes imaging[c]	2.23	0.40
Many-body optical potential[d]	2.24	0.34
Schwinger multichannel[e]	2.257	0.387
Experimental[f]	2.32	0.41

[a]Padial and Norcross, Ref. 15.
[b]Schneider and Collins, Ref. 69.
[c]Hazi *et al.*, Ref. 68.
[d]Berman and Domcke, Ref. 31.
[e]Fit to eigenphase sums from Huo *et al.*, Ref. 7.
[f]See Morgan, Ref. 65.

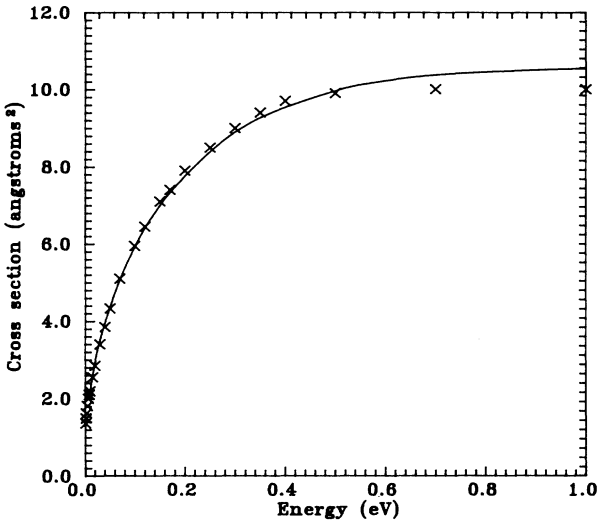

FIG. 4. Total momentum transfer cross sections calculated with the BTAD potential (solid curve) and the effective, swarm-derived experimental data of Engelhardt *et al.* (Ref. 71) (crosses).

The most recent determination of these cross sections is that of Sohn *et al.*[73] (see also Ref. 74). These authors measured absolute elastic differential cross sections from energies from 0.1 to 1.5 eV, using a crossed-beam electron spectrometer.[75] In Figs. 5, we compare theoretical and experimental elastic differential cross sections at three energies: 0.1, 0.55, and 1.5 eV. The theoretical cross sections reproduce the prominent backward scattering at the lowest energy [Fig. 5(a)]. They also exhibit the characteristic *shape* of the (*d*-wave dominated) near-resonance cross section at 1.5 eV [Fig. 5(c)]. Except at this energy, where the lack of vibrational effects in the theoretical calculation prohibits quantitative agreement, our cross sections lie only slightly outside the experimental error bars of roughly $\pm 15\%$.[76]

To effect a further comparison with the recent measurements of Sohn *et al.*,[73] we compare in Table VIII integrated elastic cross sections from our calculations and their experiment. Sohn *et al.* determined the latter by extrapolating their differential cross sections—whose measured angular range extends from 15° to 135°—to 0° and 180° and numerically integrating the result. The elastic cross section is the dominant contributor to the total cross section, so to put this comparison into perspective, we have included in Table VIII our *total* integrated cross sections at these energies as well as the measured values of Kennerly[53] and of Baldwin.[77]

3. *Rotational excitation cross sections*

Rotational excitation of nitrogen is an important energy-loss mechanism in molecular gases, and thus cross sections for this process play a significant role in the modeling of electron velocity distributions in gaseous discharges. Unlike their vibrational excitation counterparts, which for some molecules exhibit strange spikes

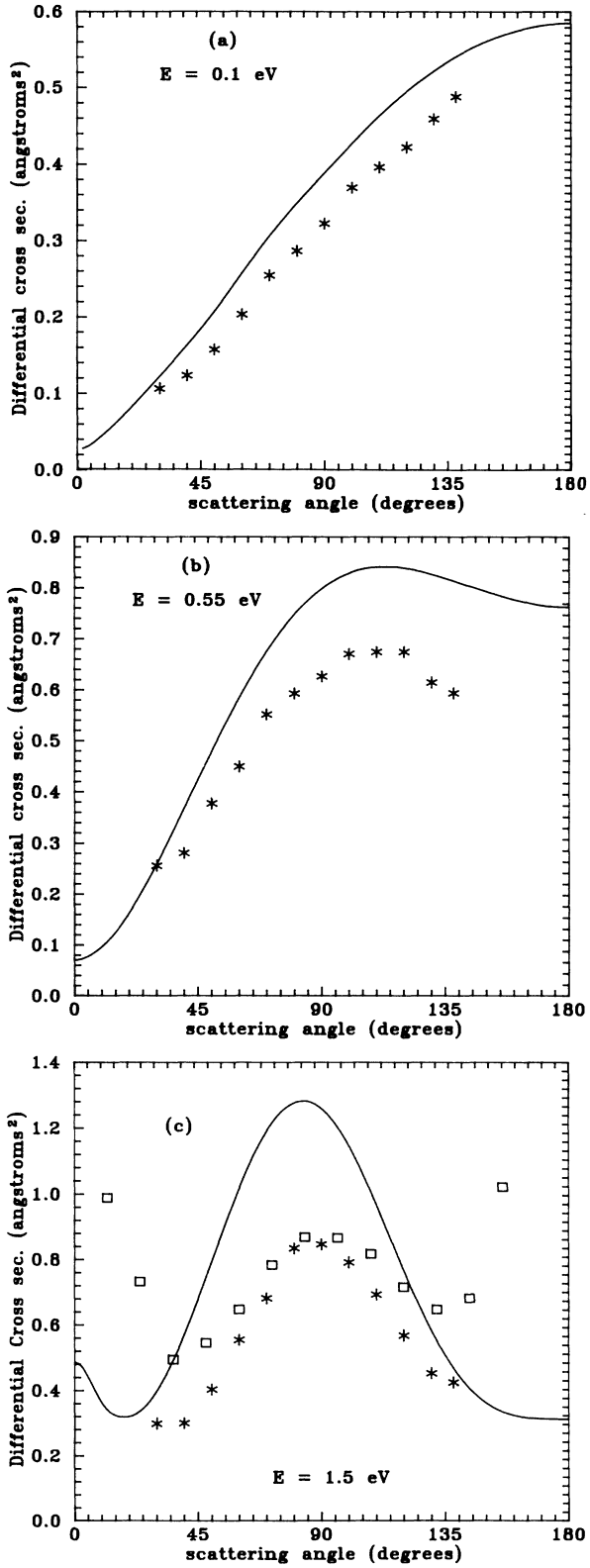

FIG. 5. Elastic e-N_2 differential cross sections at (a) 0.1 eV, (b) 0.55 eV, and (c) 1.5 eV. The solid curves are results of the present BTAD calculations. The stars are experimental data of Sohn *et al.* (Ref. 73). In (c), the squares are experimental data of Shyn and Carnignan (Ref. 74).

TABLE VIII. Integrated elastic and total e-N_2 cross sections: theoretical and experimental results. The theoretical cross sections were calculated with the BTAD potential and exact exchange at $R=2.068a_0$ (including Σ, Π, and Δ symmetries). The experimental elastic cross sections were determined by Sohn *et al.* (Ref. 73) by extrapolating and numerically integrating measured absolute differential cross sections.

	σ_{el} (Å^2)			σ_{tot} (Å^2)	
	Expt. (Ref. 73)	BTAD	BTAD	Expt. (Ref. 77)	Expt. (Ref. 53)
0.10	4.44	4.63	4.85		
0.35	6.15	7.53	7.78	6.73	
0.55	6.81	8.52	8.81	9.01	8.896
1.00	7.30	9.56	9.97	9.95	9.93
1.50	7.43	10.58	11.50	11.41	11.17

near threshold,[4] rotational excitation cross sections are usually thought to rise smoothly from threshold. A striking exception to this general precept is the e-N_2 rotational excitation cross section recently published by Onda;[78] these results show a phenomenon unique in cross sections for this process: a sharp peak at an energy near 0.08 eV.

Onda's calculations were based on the PO polarization potential of Onda and Temkin,[10] which was discussed in Sec. II A, where we noted similarities and differences between this PO potential and our BTAD potential. As is evident in Fig. 6(a), the BTAD rotational excitation cross sections exhibit the resonance peak, albeit without vibrational substructure, and $\sigma_{j_0\to j}$ for $j_0=0\to j=4$ exceeds that for $j_0=0\to j=2$ by almost a factor of 3, in confirmity with earlier findings of Burke and Chandra,[79] while cross sections for higher values of j are smaller by several orders of magnitude.[80] This behavior is similar to that seen in Onda's PO cross sections. The BTAD and PO results differ conspicuously, however, near threshold. As can be seen for $j_0=0\to j=2$ in Fig. 6(b), the former show no trace of the peak present in Onda's results. Similarly, the CP potential produces smoothly varying cross sections that, in fact, look quite like the BTAD results.

Onda's study differs from the present work in its treatment both of polarization and of exchange. Onda's calculations are based on the free-electron-gas model exchange potential introduced by Onda and Temkin[10] (see Sec. II A). This potential is scaled by an overall, multiplicative parameter ϵ that assumes two values. For the resonant (Π_g) symmetry, this parameter is given the value $\epsilon=0.482$, which positions the first resonance peak in the (oscillatory) total cross section at the experimental position measured by Kennerly.[53] In nonresonant symmetries, however, this parameter is given the value $\epsilon=0.73$, which makes the theoretical total cross section agree with Kennerly's measured result at 0.05 eV. Unfortunately, it is impossible to tell whether the disparity evident in Fig. 6(b) derives from differences in the polarization potentials used or in the treatments of exchange.

Furthermore, direct experimental resolution of this discrepancy—in, say, a crossed-beam experiment—is unlikely, considering the extremely low threshold for rotational excitation of N_2. For this molecule the rotational constant is 2.477×10^{-4} eV, so the energy spacing between the $j=0$ and levels is 0.001 486 eV.

This discrepancy may, however, be resolved by appeal to indirect techniques. Energy loss from a swarm of low-energy electrons drifting and diffusing through a gas of N_2 molecules under the influence of an applied electric field is extremely sensitive to rotational excitation cross sections. So we suggest that by feeding our rotational excitation cross sections (Table IX) and those of Onda's separately into programs that solve the Boltzmann equation to calculate transport properties such as drift velocities and diffusion coefficients and comparing those properties to measured data, one might be able to shed light on this discrepancy.[81]

A peculiarity of rotational excitation in electron swarms in N_2 is related to the two approximations to the $j_0=0\to j=2$ cross sections shown in this figure. The "quadrupole Born" cross section, calculated using the formulas of Gerjuoy and Stein,[82] are based on the first Born approximation but neglect the long-range induced polarization interaction. This interaction is included in the "polarized Born" cross section, which is based on the first Born formulas of Dalgarno and Moffett,[83] where it produces a smaller cross section than the quadrupole Born result. Interestingly, it is the *quadrupole* Born cross section—not the (presumably more accurate) polarized Born curve—that, when inserted into the multiterm solution of the Boltzmann equation, produces transport coefficients in agreement with experiment.[84] Figure 6(b) provides some insight into this observation: the BTAD and CP curves are increased over the polarized Born cross sections due to their more accurate inclusion of static, exchange, and intermediate- and short-range polarization and correlation effects. Nevertheless, all three theoretical cross sections in this figure differ significantly from the quadrupole Born curve, and it remains to be seen to what extent any of these results is consistent with existing transport data.

V. CONCLUSION

In the present research we have extended to the e-N_2 system the variationally determined nonpenetrating (BTAD) polarization potential that we originally applied to e-H_2 scattering and have compared cross sections cal-

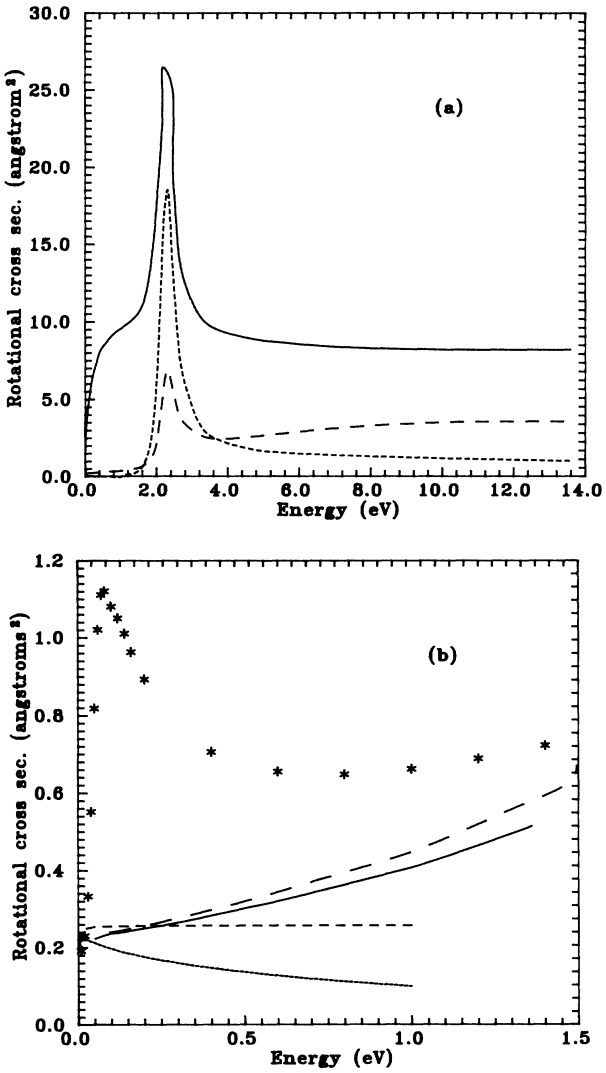

FIG. 6. Rotational excitation cross sections for e-N_2 scattering. (a) Cross sections for elastic scattering from initial state $j_0=0$ (solid curve) and for rotational excitation from this state to final states $j=2$ (long-dash curve) and $j=4$ (short-dash curve). (b) Low-energy cross sections for $j_0=0\rightarrow j=2$ from the present BTAD (solid curve) and CP (long-dash curve) calculations and from the polarized orbital study of Onda (Ref. 78) (stars). The short-dash curve was computed using the quadrupole Born approximation (Ref. 81) and the dotted curve using the polarized-Born formula (Ref. 82).

culated with this potential to a variety of experimental data. The BTAD potential appears presented in two forms convenient for future studies: tabular (Table III) and a simple analytic (fitted) function [Eqs. (21)].

The scattering calculations reported here are based on the BF-FN formulation of electron-molecule theory and include exchange effects exactly via an implementation of the linear-algebraic prescription of Schneider and Collins.[5] When used with a near-Hartree-Fock static potential, this formulation leaves three principal areas of uncertainty: (i) the target is uncorrelated; (ii) vibrations of the target are excluded, and (iii) polarization effects are treated approximately. The focus of the present study is on the last of these matters.

TABLE IX. Low-energy theoretical rotational excitation e-N_2 cross sections $\sigma_{j_0\rightarrow j}$ (in square angstroms) based on FN T matrices calculated with the BTAD potential and exact exchange at $R=2.068a_0$ (including Σ, Π, and Δ symmetries). These data were determined via the adiabatic nuclear rotation theory (see Sec. IV C 3). Only results for energies below 1.0 eV are shown, but a more complete table, including energies up to 13.6 eV, is available on request from the authors. ($1.0[-04]=1.0\times10^{-4}$.)

E (eV)	$\sigma_{0\rightarrow0}$	$\sigma_{0\rightarrow2}$	$\sigma_{0\rightarrow4}$	$\sigma_{0\rightarrow6}$
0.0100	1.711	0.121	0.827[−03]	
0.0200	2.265	0.199	0.864[−03]	0.632[−04]
0.0300	2.704	0.219	0.671[−03]	0.648[−04]
0.0400	3.070	0.222	0.458[−03]	0.583[−04]
0.0500	3.393	0.222	0.399[−03]	0.104[−03]
0.0600	3.684	0.225	0.300[−03]	0.966[−04]
0.0700	3.950	0.229	0.240[−03]	0.893[−04]
0.0800	4.195	0.232	0.202[−03]	0.811[−04]
0.1000	4.633	0.236	0.715[−04]	0.147[−04]
0.1360	5.287	0.240	0.714[−04]	0.494[−05]
0.1500	5.508	0.242	0.775[−04]	0.616[−05]
0.2720	6.923	0.260	0.197[−03]	0.273[−05]
0.3500	7.527	0.274	0.432[−03]	0.238[−05]
0.5500	8.524	0.311	0.236[−02]	0.992[−06]
0.6800	8.928	0.337	0.574[−02]	0.762[−06]
1.0000	9.565	0.407	0.349[−02]	0.200[−05]

The comparisons in Figs. 2–5 of theoretical and experimental integrated total and momentum transfer cross sections and of differential elastic cross sections show that the BTAD potential consistently yields results in excellent agreement with existing data. Rotational excitation, however, remains a source of concern, in light of the significant differences evident in Fig. 6 between the BTAD cross sections and the PO results of Onda.[78]

Within the context of these BTAD studies, we have also examined two other model polarization potentials—the CP potential of O'Connell and Lane[14] and the parameter-dependent phenomenological form (7)—in numerically and physically consistent scattering calculations.

We have confirmed the observations of Padial and Norcross[15] that the CP potential produces cross sections in excellent agreement with experimental data and have compared this potential and the cross sections it yields to those of our (quite different) variational nonpenetrating model. In this regard, we note that the CP model is by far the simplest of existing parameter-free models to calculate.

An important, as-yet-unresolved question concerning the CP potential concerns its accuracy in calculations of cross sections for *vibrational excitation*. The only existing study to directly address this question is that of Morrison and Saha,[51] who used the BTAD and CP po-

tentials to calculate vibrational excitation e-H_2 cross sections. Their finding—that e-H_2 cross sections exhibit high sensitivity to the polarization component of the interaction potentials—argues for similar investigations on other systems, and we have made tests of the CP potential a part of our forthcoming study of vibrational excitation of N_2.

Indeed, the primary limitation of the present calculations is probably our imposition of the rigid-rotator approximation, which prohibits vibrations of the target and its dynamical interaction with the projectile. To rectify this shortcoming we are currently generating BTAD potentials for a range of internuclear geometries for use in calculations of vibrational excitation and other cross sections.

ACKNOWLEDGMENTS

We owe a great debt to Dr. Lee A. Collins and Dr. Barry I. Schneider, who provided a prototype of the linear-algebraic program used in these calculations and who gave us the benefit of their advice at several stages in this project. We would also like to thank Dr. David Norcross and Dr. Steve Alston for sometimes lengthy but always valuable conversations concerning the CP and BTAD potentials, Dr. A. Temkin for sending us tables of his PO potentials, Dr. V. McKoy and Dr. W. Huo for providing tables of their Schwinger multichannel results, Dr. Diane L. Lynch for invaluable assistance during an early stage of this research, Mr. K. B. Chan for work on the analytic fit to our BTAD potential, Dr. Robert Crompton and Dr. Gerry Haddad for advice concerning the contrariety in Fig. 6, and Dr. K. Jung for examining and commenting on the comparisons in Figs. 5. We also are grateful to Dr. Thomas M. Miller for researching the latest information on the experimental polarizabilities of N_2 and to the many people who critiqued this manuscript in various earlier versions: Wayne Trail, Mehran Abdolsalami, and Dr. Norcross, Dr. Collins, Dr. Miller, and Dr. Andy Feldt. This research supported by Grant No. PHY-8505438 from the National Science Foundation, to whom we are most grateful.

[1]A. V. Phelps. in *Electron-Molecule Scattering,* edited by S. C. Brown (Wiley, New York, 1979), Chap. 1.
[2]G. J. Schulz, Rev. Mod. Phys. **45**, 423 (1973).
[3]N. F. Lane, Rev. Mod. Phys. **52**, 29 (1980).
[4]M. A. Morrison, Aust. J. Phys. **36**, 239 (1983).
[5]B. I. Schneider and L. A. Collins, Phys. Rev. A **27**, 2847 (1983).
[6]P. G. Burke, C. J. Noble, and S. Salvini, J. Phys. B **16**, L113 (1983).
[7]W. Huo, T. L. Gibson, M. A. P. Lima, and V. McKoy, Phys. Rev. A **36**, 1632 (1987).
[8]B. I. Schneider, Phys. Rev. A **31**, 2188 (1985).
[9]N. F. Lane and R. J. W. Henry, Phys. Rev. **173**, 183 (1968).
[10]K. Onda and A. Temkin, Phys. Rev. A **28**, 621 (1983).
[11]T. L. Gibson and M. A. Morrison, Phys. Rev. A **29**, 2497 (1984).
[12]A. Temkin, Phys. Rev. **107**, 1004 (1957).
[13]A. Temkin, and J. C. Lamkin, Phys. Rev. **121**, 788 (1961).
[14]J. O'Connell and N. F. Lane, Phys. Rev. A **27**, 1893 (1983).
[15]N. T. Padial and D. W. Norcross, Phys. Rev. A **29**, 1742 (1984).
[16]N. T. Padial and D. W. Norcross, Phys. Rev. A **29**, 1590 (1984); N. T. Padial, *ibid.* **32**, 1379 (1985); A. Jain and D. W. Norcross, *ibid.* **32**, 134 (1985); J. Chem. Phys. **84**, 739 (1986); P. K. Bhattacharyya, D. K. Syamal, and B. C. Saha, Phys. Rev. A **32**, 854 (1985).
[17]S. Hara, J. Phys. Soc. Jpn. **27**, 1262 (1969).
[18]M. A. Morrison, Adv. At. Mol. Phys. (to be published).
[19]In atomic units, $\hbar = m_e = e = a_0 = 1$. The unit of energy is $\hbar^2/m_e a_0^2 = 1$ hartree $= 1E_h = 2$ Ry $= 27.212$ eV. The unit of distance is the first Bohr radius $a_0 = 1$ Bohr $= 0.529\,18 \times 10^{-10}$ m.
[20]L. Castillejo, I. C. Percival, and M. J. Seaton, Proc. R. Soc. London, Ser. A **254**, 259 (1969).
[21]T. L. Gibson. Ph.D. thesis, University of Oklahoma, 1982.
[22]M. A. Morrison and P. J. Hay, Phys. Rev. A **20**, 740 (1979).
[23]R. A. Eades, D. A. Dixon, and D. G. Truhlar, J. Phys. B **15**, 2265 (1982).
[24]J. W. Moskowitz and L. C. Snyder, in *Methods of Electronic Structure Theory,* edited by H. F. Schaeffer III (Plenum, New York, 1977), p. 387.
[25]S. Hara, J. Phys. Soc. Jpn. **22**, 710 (1967).
[26]M. A. Morrison and L. A. Collins, Phys. Rev. A **17**, 918 (1978).
[27]T. L. Gibson and M. A. Morrison, J. Phys. B **14**, 727 (1981).
[28]W. E. Weitzel III, T. L. Gibson, and M. A. Morrison, Comput. Phys. Commun. **30**, 151 (1983).
[29]E. C. Sullivan and A. Temkin, Comput. Phys. Commun. **25**, 97 (1982); A. Temkin, in *Proceedings of the Symposium on Electron-Molecule Collisions,* edited by I. Shimamura and M. Matsuzawa (University of Tokyo, Tokyo, 1979), p. 97.
[30]C. A. Weatherford, K. Onda, and A. Temkin, Phys. Rev. A **31**, 3620 (1985).
[31]M. Berman and W. Domcke, J. Phys. B **17**, L453 (1984).
[32]A. Temkin and K. V. Vasavada, Phys. Rev. **160**, 190 (1967); A. Temkin, K. V. Vasavada, E. S. Chang, and A. Silver, *ibid.* **186**, 57 (1969).
[33]D. M. Chase, Phys. Rev. **104**, 838 (1956); E. S. Chang and U. Fano, Phys. Rev. A **6**, 173 (1972); M. Shugard and A. U. Hazi, *ibid.* **12**, 1895 (1975).
[34]M. A. Morrison, A. N. Feldt, and D. A. Austin, Phys. Rev. A **29**, 2518 (1984).
[35]In its application to rotational excitation for e-H_2 scattering, the ANR approximation introduces errors as great as 30% at near-threshold energies (see Ref. 34). But we expect the errors for the corresponding e-N_2 scattering process to be much smaller than this, because the rotational constant for nitrogen, $B_{\rm rot} = 1.998$ cm^{-1} is considerably smaller than its counterpart for H_2, $B_{\rm rot} = 60.85$ cm^{-1}.
[36]M. A. Morrison, Comput. Phys. Commun. **21**, 63 (1980); L. A. Collins, D. W. Norcross, and G. B. Schmid, *ibid.* **21**, 79 (1980).
[37]M. E. Rose, *Elementary Theory of Angular Momentum* (Wiley, New York, 1957).

[38]M. A. Morrison and G. A. Parker, Aust. J. Phys. **40**, 465 (1987).
[39]T. N. Rescigno and A. E. Orel, Phys. Rev. A **24**, 1267 (1981); L. A. Collins and B. I. Schneider, *ibid.* **34**, 1564 (1986).
[40]S. Huzinaga, J. Chem. Phys. **42**, 1293 (1965).
[41]T. Dunning, J. Chem. Phys. **55**, 3958 (1971).
[42]This value differs slightly from that of Ref. 22 because Morrison and Hay included only the 36 most important of the 40 possible symmetrized molecular orbitals that can be constructed from the $(6s5p2d)$ neutral basis. We redid these Hartree-Fock calculations using all 40 orbitals.
[43]P. A. Christiansen and E. A. McCullough, Jr., J. Chem. Phys. **55**, 439 (1978).
[44]These moments are somewhat sensitive to the basis used in the HF calculation of the $X\,^1\Sigma_g^+$ wave function. For example, the static potential calculated using the basis of Cade *et al.* (Ref. 45), which is constructed from Slater-type orbitals, gives $c_2=-0.9379ea_0^2$, $c_4=-6.8135ea_0^4$, and $c_6=-11.7522ea_0^6$.
[45]P. E. Cade, K. D. Sales, and A. C. Wahl, J. Chem. Phys. **44**, 1973 (1966).
[46]G. Herzberg, *Molecular Spectra and Molecular Structure. I Spectra of Diatomic Molecules,* 2nd ed. (Van Nostrand, New York, 1950).
[47]N. J. Bridge and A. D. Buckingham, Proc. R. Soc. London, Ser. A **295**, 334 (1966).
[48]A. C. Newell and R. C. Baird, J. Appl. Phys. **36**, 3751 (1965).
[49]R. H. Orcutt and R. H. Cole, J. Chem. Phys. **46**, 697 (1967).
[50]T. M. Miller and B. Bederson, Adv. At. Mol. Phys. **13**, 1 (1978).
[51]M. A. Morrison, and B. C. Saha, Phys. Rev. A **34**, 2786 (1986).
[52]The slight differencess between our parameters and those reported by Padial and Norcross (Ref. 15) for e-N_2 with $R=2.068a_0$ derived from three sources. First, our basis differs slightly from that of Cade *et al.* (Ref. 45), which was used by Padial and Norcross. Second, the form we used for the correlation potential differs from the one used by these authors [compare Eqs. (6) and (9) of Ref. 15]. Finally, Padial and Norcross used experimental polarizabilities, while we used the values extracted from our BTAD potential [see Eq. (19)].
[53]R. E. Kennerly, Phys. Rev. A **21**, 1876 (1980).
[54]J. Light and R. B. Walker, J. Chem. Phys. **65**, 4272 (1976).
[55]L. A. Collins and B. I. Schneider, Phys. Rev. A **24**, 2387 (1981).
[56]J. Callaway, R. W. LaBahn, R. T. Pu (Poe), and W. M. Duxler, Phys. Rev. **168**, 12 (1968).
[57]C. J. Noble, P. G. Burke, and S. Salvini, J. Phys. B **15**, 3779 (1982).
[58]H.-D. Meyer, Phys. Rev. A **34**, 1979 (1986).
[59]L. A. Collins, W. D. Robb, and M. A. Morrison, Phys. Rev. A **21**, 488 (1980).
[60]L. A. Collins (private communication); this calculation was based on the N_2 wave function of Ref. 45.
[61]S. Trajmar, D. F. Register, and A. Chutjian, Phys. Rep. **97**, 221 (1983).
[62]O. Suoeka and S. Mori, J. Phys. Soc. Jpn. **53**, 2491 (1984).
[63]Our CP results differ slightly from those reported by Padial and Norcross (Ref. 15). For example, at $E_b=0.01$ Ry, their Σ_g eigenphase sums and partial cross sections are 3.0331 rad and $14.339a_0^2$, respectively; our CP results at this energy are 3.0246 rad and $16.2669a_0^2$. We attribute these differences to the disparities between the two studies noted in Ref. 52.
[64]N. Chandra and A. Temkin, Phys. Rev. A **14**, 507 (1976).
[65]L. A. Morgan, J. Phys. B **19**, L439 (1986).
[66]B. I. Schneider, M. Le Dourneuf, and Vo. Ky Lan, Phys. Rev. Lett. **43**, 1926 (1979).
[67]L. Dubé and A. Herzenberg, Phys. Rev. A **20**, 194 (1979).
[68]A. Hazi, T. N. Rescigno, and M. Kurilla, Phys. Rev. A **23**, 1089 (1981).
[69]B. I. Schneider and L. A. Collins, Phys. Rev. A **30**, 95 (1984).
[70]M. Berman, H. Estrada, L. S. Cederbaum, and W. Domcke, Phys. Rev. A **28**, 1361 (1983).
[71]A. G. Engelhardt, A. V. Phelps, and C. G. Risk, Phys. Rev. **135**, A1566 (1964).
[72]A. V. Phelps and L. A. Pitchford, Phys. Rev. A **31**, 2932 (1985).
[73]W. Sohn, K.-H. Kochem, K.-M. Scheuerlein, K. Jung, and H. Erhardt, J. Phys. B **19**, 4017 (1987).
[74]T. W. Shyn and G. R. Carnignan, Phys. Rev. A **22**, 923 (1980).
[75]K.-H. Kochem, W. Sohn, N. Hebel, K. Jung, and H. Ehrhardt, J. Phys. B **18**, 4455 (1985).
[76]K. Jung (private communication).
[77]G. C. Baldwin, Phys. Rev. A **9**, 1225 (1974).
[78]K. Onda, J. Phys. Soc. Jpn. **54**, 4544 (1985).
[79]P. G. Burke and N. Chandra, J. Phys. B **5**, 1696 (1972).
[80]The rotational excitation cross sections reported in this paper were computed from the BF-FN T matrices by application of the adiabatic-nuclear-rotation theory (Refs. 32 and 33). For excitations in N_2, the extremely small energy separation between adjacent rotational levels means that this approximation will probably be quite accurate for this system (see Ref. 35).
[81]For this purpose, cross sections for excitations other than those in Table IX will be needed. Fortunately, the extremely small rotational energy spacing in N_2 justifies use of simple scaling ratios derived from adiabatic-nuclear-rotation theory to calculate these data [see I. Shimamura, in *Electron-Molecule Collisions,* edited by I. Shimamura and K. Takayanagi (Plenum, New York, 1984)].
[82]E. Gerjuoy and S. Stein, Phys. Rev. **97**, 1671 (1955).
[83]A. Dalgarno and R. J. Moffett, Proc. Nat. Acad. Sci. India **33**, 511 (1963).
[84]G. Haddad (private communication).